Journal of Alloys and Compounds 509 (2011) 10145–10149

Contents lists available at SciVerse ScienceDirect

Journal of Alloys and Compounds

journal homepage: www.elsevier.com/locate/jallcom

A simple wet-chemical approach to synthesize shape controlled high magnetic moment Fe_{71}–Co_{29} nanocrystals

G. Suresh, D. Rajan Babu*

School of Advanced Sciences, VIT University, Vellore 632014, India

ARTICLE INFO

Article history:
Received 25 June 2011
Received in revised form 10 August 2011
Accepted 11 August 2011
Available online 22 August 2011

Keywords:
Intermetallics
Chemical synthesis
Precipitation
Magnetic measurements
SEM

ABSTRACT

Spherical Fe_{71}–Co_{29} nanocrystals functionalized by trisodium citrate (TSC) have been synthesized using co-precipitation process. The synthesized nanocrystals have disordered structure, reductive hydrogen annealing at 450 °C has transformed the disordered phase to body centered cubic phase (CsCl structure) without secondary phases which was subsequently authenticated using Rietveld refinement technique. The TSC adhere with the Fe–Co nanocrystal's surface by carboxylate chemisorption which has been confirmed using FT-IR spectroscopy. Back scattered electron microscope image confirms the spherical morphology with size around 20 nm. The observed saturation magnetization is as large as 95.6% of bulk (242 emu g^{-1}) which is a significant indication for the crystallization of single phase Fe_{71}–Co_{29} nanocrystals.

1. Introduction

Synthesis of magnetic nanoparticles aroused intense research interest owing to its variety of sophisticated applications in various engineering and biomedical applications such as ultrahigh density data storage [1], ferrofluids [2], catalysis [3], magnetic resonance imaging [4], magnetic hyperthermia treatment [5] and radio frequency applications [6], electromagnetic wave observer [7], etc. Among all the binary transition metal alloys known, Fe–Co alloys possess a unique combination of high saturation magnetization (M_s), high Curie temperature, low magnetocrystalline anisotropy and good strength. Fe–Co alloy plays a vital role in applications requiring soft magnetic materials and they are ideally suited for applications requiring high flux densities [8]. It is worth noting the M_s of Fe_{72}–Co_{28} bulk alloy is 242 emu g^{-1} [9,10]. Combinations of properties such as large permeability, low coercivity (H_c) and large M_s have driven this alloy for variety of sophisticated applications. The Fe–Co alloy nanocrystals have been demonstrated to possess superior properties, particularly the permeability at the broad microwave range [11]. More recently, this material has shown to be an excellent soft magnetic material at nano regime for sophisticated soft magnetic applications such as radio frequency inductors for portable communication devices [6].

The major challenges faced in the chemical synthesis of Fe–Co nanocrystals are (i) crystallization of mixed phases, i.e. body centered cubic (bcc) and oxide phases when the atomic ratio of Fe:Co precursors is more than two [12]. It is worth noting that (M_s = 242 emu g^{-1}) [9,10] is attained only at Fe_{72}–Co_{28} (when the atomic ratio of Fe:Co is ≈ 2.5) and (ii) its poor chemical stability, i.e. as-synthesized samples of Fe–Co alloy nanocrystals quickly oxidize and diminish M_s, (iii) secondary crystallization such as fcc-cobalt [4]. In order to stabilize and to achieve the crystallographic phase from poorly crystalline to bcc structure of bulk alloy, the samples are heated in inert (argon or hydrogen or in mixed) atmosphere. High temperature annealing process is one of the crucial steps in inducing the crystallization in nanomaterials which relieves the imparted stress in the as prepared nanoparticles, at higher annealing temperatures the atomic mobility increases allowing the removal of stress and defects [13,14]. The annealing process may also induce secondary crystallization, hence careful selection of annealing temperature is very essential, because crystallographic phases play a major role in influencing the magnetic properties.

In the present study, we have selected the facile co-precipitation technique to synthesize and to succeed in preparing single phase Fe–Co alloy nanocrystals. In order to fabricate magnetic alloy nanoparticles, it is most important that the synthesized nanocrystals have the proper composition and crystal structure resembling the bulk. So the composition has been tailored to attain the expected magnetic property and precursors were charged in the reaction as desired. This article reports the chemical synthesis and

* Corresponding author. Tel.: +91 416 220 2804; fax: +91 416 224 3092.
E-mail addresses: drajanbabu@vit.ac.in, rajanbabud@hotmail.com (D. Rajan Babu).

0925-8388/$ – see front matter © 2011 Elsevier B.V. All rights reserved.
doi:10.1016/j.jallcom.2011.08.064

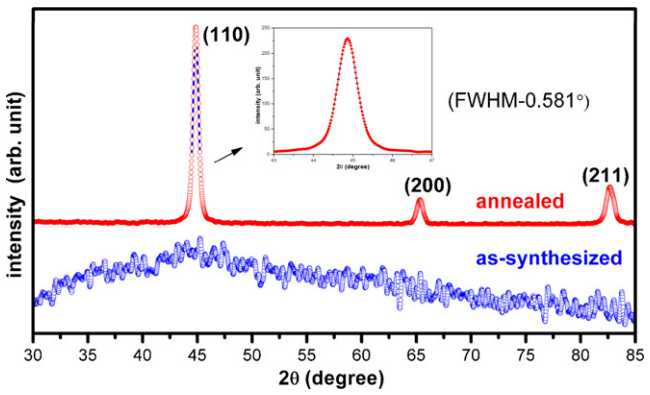

Fig. 1. X-ray diffraction pattern of as-synthesized and annealed Fe–Co nanoparticles, inset figure shows the FWHM of annealed sample.

characterization of wet-chemically synthesized Fe–Co nanocrystals in detail.

2. Materials and method

All the chemicals were procured from commercial sources with ultra high purity. In a typical synthesis, 2.8 mmol of iron sulfate heptahydrate, 1.2 mmol of cobalt chloride hexahydrate and 0.4 mmol of trisodium citrate (TSC) dihydrate were dissolved in 500 ml deionized water with vigorous stirring. The dissolved precursors were purged with 99.99% nitrogen gas (N_2) to eliminate the dissolved molecular oxygen. In 20 ml of deionized, deoxygenated water 7.64 mmol of sodium borohydride was dissolved and added very slowly to the precursors using silicone septum-syringe arrangement and allowed to stir for 10 min at room temperature [14]. The resultant was magnetically separated and washed with deionized and deoxygenated water. The resultant has been stored in ethanol for further characterizations [15]. The sample was annealed in hydrogen (H_2 gas) atmosphere at 450 °C and then the structural and magnetic properties were studied.

2.1. Characterizations

X-ray diffraction (XRD) patterns were recorded in Bruker D8 Advance diffractometer equipped with Ni filter and operated at 40 kV, 30 mA (Cu $K\alpha_1$ radiation). Thermo gravimetric analysis (TGA) was done in TA Instrument, USA/SDT Q600 in the nitrogen atmosphere equipped with Thermal Advantage software with the heating rate of 5 °C/min. Atomic absorption spectroscopy (AAS) measurement was carried out in Varian Spectra A240. Field Emission-Scanning Electron Microscopy (FE-SEM) imaging was observed in FEI Quanta FEG 200. Vibrating sample magnetometer (VSM) measurement was carried out in Lakeshore VSM 7410 with the maximum applied field of 20,000 Oe.

2.2. Data collection for Rietveld refinement

When the sample was prepared for XRD data collection, annealed sample was dusted on a greased silicon (zero background) sample holder carefully in order to remove the possible preferred orientation. Data was collected with 0.02° steps in the range of 30–85°. A total of 3000 points were collected for the total angular range. The structural model and initial structural parameters for the sample were taken as follows: space group $Im\bar{3}m$; diffraction profiles has been modelled using multiterm Simpson's rule integration of the pseudo-Voigt function. Each structural model has been refined to convergence; the best result was selected on the basis of agreement factors. The fitting quality of the experimental data was checked by using the following parameters: the goodness of fit (S) must tend to 1 and two reliability factors, R_p and R_{wp} (weighted differences between measured and calculated values) must be close to or less than 10% [16,17]. The Rietveld refinement was carried out using GSAS software [18].

3. Results and discussion

Fig. 1 shows the XRD pattern of as-synthesized and annealed samples. The XRD pattern of as-synthesized sample does not give any diffraction peaks; only a broad hump is observed around 45°, which is probably due to the lower crystallinity and strong surface effects due to the small size of the synthesized particles [19]. Fig. 2 shows the TGA pattern of the sample. From the pattern, a gradual loss in weight is observed from 28 °C to 415 °C which corresponds to the decomposition of citrate [20]. The observed

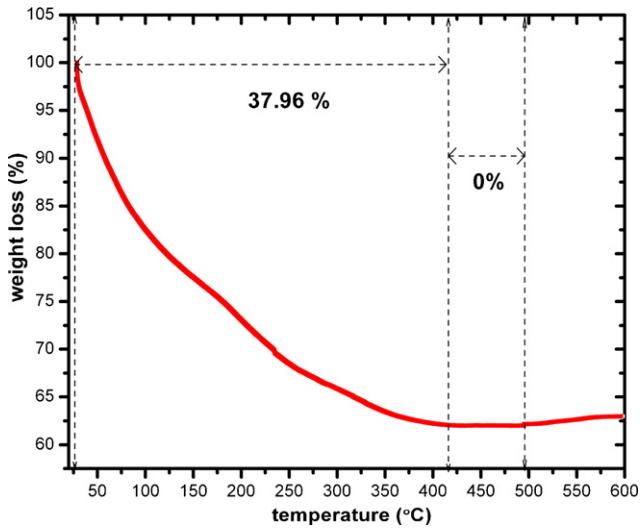

Fig. 2. TGA trace of as-synthesized Fe–Co nanoparticles.

Table 1
Crystallographic data of Fe–Co alloy.

Parameter	Fe–Co [21]
a (Å)	2.867
Space group	$Im\bar{3}m$
Volume (Å^3)	23.12
Density (g/cm^3)	8.18
Z (unit cell content)	2
x	0
y	0
z	0
occ	1

weight loss from 420 °C to 496 °C is almost negligible which denotes the complete decomposition of the citrate moiety. So the annealing process was carried out at 450 °C for about 30 min to attain the required crystallographic phase as-well as to avoid the secondary phase crystallization. The analysis of TGA data reveals that the total weight loss of the sample is found to be 37.96%. The annealing process enhanced the crystallinity of the sample as well as it created a carbonaceous coating on the surface of the particles which protects them from oxidation [19]. The XRD pattern of annealed sample which is shown in Fig. 1 gives sharp diffraction peaks at 44.815°, 65.329° and 82.699°. The inset of Fig. 1 shows the full width half maximum (FWHM) of 0.581°. The crystallite size has been calculated using Scherrer formula which is 16.36 nm. The Rietveld refinement has been carried out with initial positional parameters as given in Table 1 [21]. Fig. 3 shows the Rietveld refined XRD pattern and the refined parameters are listed in Table 2. Successful refinement of 20 variables have resulted in the decrease of lattice parameters from 2.867 Å to 2.860 Å, which is an

Table 2
Rietveld refined parameters.

Parameter	Rietveld refined
Crystal system	bcc
Space group	$Im\bar{3}m$
a (Å)	2.860
Volume (Å^3)	23.4
Density (g/cm^3)	7.926
Z (unit cell content)	2
R_{wp} (%)	11.85
R_p (%)	7.53
S (goodness of fit = R_{wp}/R_p)	1.573
χ^2	9.624

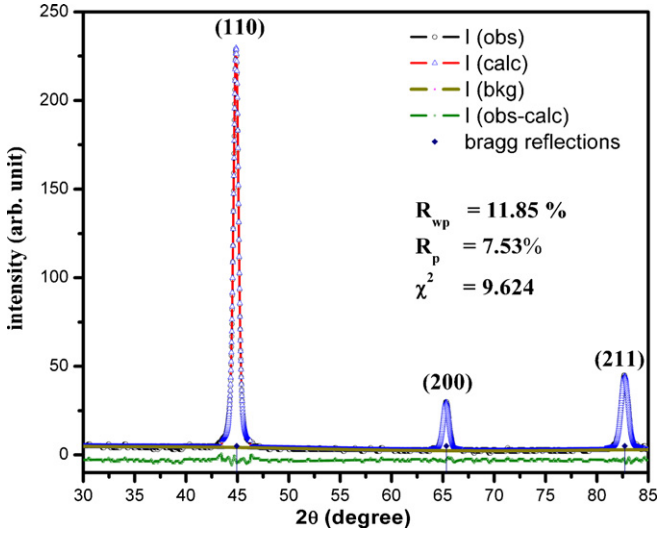

Fig. 3. Rietveld refined XRD pattern of annealed Fe–Co nanoparticles.

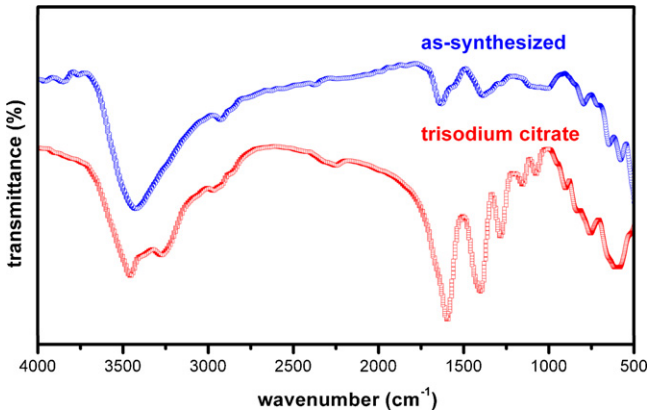

Fig. 4. FT-IR spectra of trisodium citrate and as-synthesized sample.

indication in the shift of diffraction peaks towards lower angle side which means that *d*-spacing value increases with the cobalt substitution. This is due to the fact that iron has larger atomic radius than that of cobalt, and it confirms that cobalt atoms are substituted in the iron matrix and forms the bcc phase, which is convincible by the reliability factors of Rietveld refinement (S, R_p, R_{wp} and χ^2) these reliability factors are in acceptable limit [16] and are listed in Table 2. FT-IR spectroscopy has been used to study the functionalization of the nanocrystals with stabilizing molecules. FT-IR spectra of Fe–Co nanoparticles functionalized with TSC and TSC is shown in Fig. 4, which prove the creation of chemical bonds between C and O atoms with nanoparticle's surface through carboxylate chemisorption [22] which is stabilized electrostatically due to citrate anion adsorption on the surface of the nucleated seeds [23]. Citrate is a weak reducing agent as-well as an anionic surfactant [24]. The detailed analysis of the FTIR spectra reveals the nature of TSC binding with nanoparticle's surface. The observed bond vibrations are listed in Table 3. The large and intense band observed around 3400 cm^{-1} could be assigned to O—H stretching

Table 3
FT-IR bond vibrations.

Wave number (cm^{-1})	Bond vibration
3400	O—H stretching
1644	C═O stretching
1400	C—O asymmetric stretching

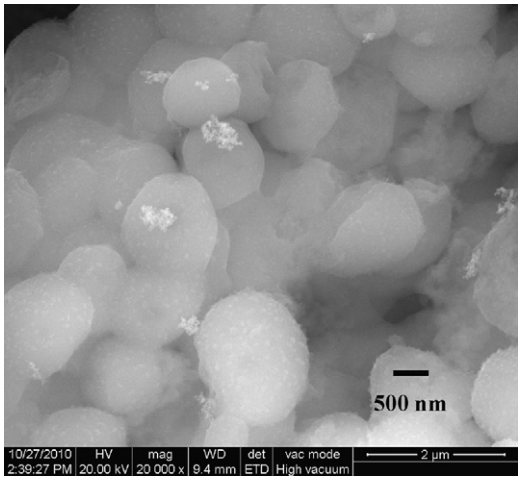

Fig. 5. FE-SEM image of spherical granules composed of Fe–Co nanocrystals.

and the bond vibration observed at 1600 cm^{-1} can be assigned to C═O vibration of citrate. When TSC has bound with nanocrystals surface, this C═O bond vibration shifts to 1644 cm^{-1} in TSC stabilized Fe–Co nanocrystals and render C═O bond a partial single bond character [25]. The band observed around 1400 cm^{-1} of citrate could be assigned to asymmetric stretching of C—O from the COOH group. TSC binds with Fe–Co nanocrystals with two of its three carboxylic groups associating with the nanocrystals. The nucleophilic adsorption of the carboxylic anions causes fraction of electron transfer to the host particle. The third anion is remains in the solution [26]. The adsorption of carboxylic group to the nanocrystals surface is witnessed by the bond vibration shift from 1400 cm^{-1} to 1393 cm^{-1}. It can also be observed from the spectrum that the bond vibration has become weak. From these observations, it is explicit that the nanocrystals are functionalized by citrate through the carboxylic group adsorption. The measurement of atomic composition using AAS confirms the composition to be Fe_{71}–Co_{29} which is in good agreement with the charged precursor. Fig. 5 shows the FE-SEM image of Fe–Co granules composed of nanocrystals. Fig. 6 shows the FE-SEM image at higher magnification, where the spherical nanocrystals with size around 20 nm could be observed. These nanocrystals are almost spherical in shape. The aggregation of nanocrystals observed in the FE-SEM image is due to the dipolar interaction of the nanocrystals [27] apart from the enormous surface energy. The crystallite size

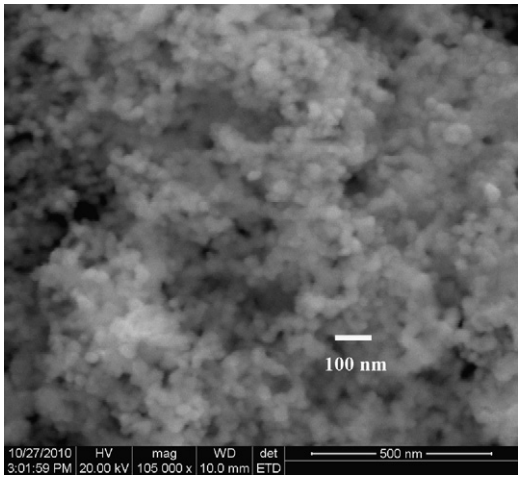

Fig. 6. FE-SEM image of Fe–Co nanocrystals.

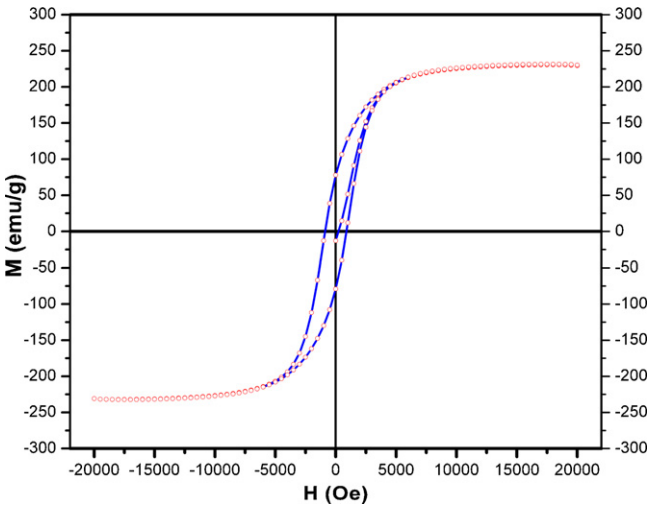

Fig. 7. *M–H* loop of annealed Fe–Co nanoparticles.

(16.26 nm) calculated using Scherrer formula is in good agreement with FE-SEM image. The VSM measurement shows ferromagnetic behaviour at room temperature which is shown in Fig. 7 with M_s and H_c of 231.46 emu g^{-1} and 800 Oe respectively. The M_s of Fe_{72}–Co_{28} bulk alloy is 242 emu g^{-1} [9,10] and it depends on the ratio of iron and cobalt atoms [28] as well as on the crystallographic phases [4]. The M_s in principle should be directly proportional to the number of magnetic atoms in the particle. The M_s can be explained with the help of Slater–Pauling curve by polarization of *d* band [29,30]. We have observed the highest M_s value of 231.46 emu g^{-1} for Fe_{71}–Co_{29} nanocrystals which is very near to the maximum value of bulk Fe_{72}–Co_{28} alloy [9,10]. The observed M_s in Fe_{71}–Co_{29} nanocrystals is greater than that of the bulk iron metal, which is also an indication of the formation of the alloy nanocrystals with largest Fe composition (i.e. Fe: Co atomic ratio ~2.5). The M_s of iron (bulk) is 222 emu g^{-1} and cobalt (bulk) is 162 emu g^{-1} [31,32]. The obtained M_s manifests the formation of single phase bcc Fe–Co alloy which has been confirmed by Rietveld refinement. But, the observed M_s of Fe_{71}–Co_{29} alloy nanocrystals (231.46 emu g^{-1}) is less than the bulk (242 emu g^{-1}), which may be due to the reasons such as (i) the M_s of Fe_{72}–Co_{28} alloy (242 emu g^{-1}) reported by Slater–Pauling curve was calculated at −273 °C [31] and (ii) the reduction of the particle size results in a large fraction of atoms on the surface of the particle and these atoms have a few nearest neighbours to which they can interact. Therefore, it is more likely that their moment become randomly oriented at the surface (spin-canting) [33]. The H_c of the synthesized Fe–Co nanocrystals is 800 Oe which agrees well with the literature [34,35], which may be due to the relationship between the H_c and the grain size (D) of nanostructured soft magnetic alloys which was proposed by Herzer [36]. This model is widely accepted to describe most of the nanocrystalline alloys accurately using $H_c \propto D^6$ power law relationship [36,37]. The other reason for the attained H_c may be due to multi magnetic to single domain transition, (i.e. a single domain is the critical size in which the largest H_c occurs) [32,38,39] which may be due to the fact that the collinear arrangement of spins in the nanocrystals are nearer to the superparamagnetic limit [40]. It is noteworthy, that the superparamagnetic size limit of Fe–Co nanocrystals is around 6 nm [28,41]. It is remarkable that we have observed the combination of large M_s as well as moderate H_c in a soft magnetic material. Combination of properties such as large M_s and moderate H_c will eventually drive these materials for sophisticated applications.

4. Conclusions

In summary, high magnetic moment Fe_{71}–Co_{29} alloy nanocrystals have been synthesized using a simple and inexpensive co-precipitation technique followed by the reductive H_2 annealing with negligible oxide formation and can be synthesized in large yield. The post-thermal treatment induces crystallization from amorphous to bcc phase, as-well as it has created a carbonaceous coating on the sample which protects it from oxidation. The Rietveld refinement confirms the formation of (bcc) single phase and lattice parameters have been calculated. The reliability factors of Rietveld refinement end up with the convincible values of (R_{wp} = 11.85%, R_p = 7.53%, S = 1.573 and χ^2 = 9.624). The citrate anions bind with nanocrystals with two of its three carboxylic groups. The nucleophilic adsorption of the carboxylic anions causes fraction of electron transfer to the host and functionalizes the Fe–Co nanocrystals. The morphology and size of the nanocrystals has been measured using FE-SEM, which shows the spherical nature and confirms the size of the particles around 20 nm which agrees very well with the crystallite size calculated using Scherrer formula. The high M_s (231.46 emu g^{-1}) is one of the major indications of the formation of single phase bcc-Fe–Co nanocrystals which is subsequently supported by the Rietveld refinement. The probable reason for the observed H_c could be the grain size dependence of nanocrystalline alloys and also the collinear arrangement of spins of the nanocrystals near the superparamagnetic size limit. Synthesis of materials using facile process with combination of properties of soft and hard magnetic materials will eventually drive these materials into sophisticated applications.

Acknowledgements

One of the authors G.S. gratefully acknowledges the financial support awarded by the Management, VIT University, Vellore 632 014, India through the Research associateship and also for the technical discussions with Dr. P. Saravanan, Scientist-D, Defence Metallurgical Research Laboratory, Hyderabad-500058, India.

References

[1] S. Sun, C.B. Murray, D. Weller, L. Folks, A. Moser, Science 287 (2000) 1989–1992.
[2] M. Zahn, J. Nanopart. Res. 3 (2001) 73–78.
[3] C. Che, W. Li, S. Lin, J. Chen, J. Zheng, J.-c. Wu, Q. Zheng, G. Zhang, Z. Yang, B. Jiang, Chem. Commun. (2009) 5990–5992.
[4] W.S. Seo, J.H. Lee, X. Sun, Y. Suzuki, Davidmann, Z. Liu, M. Terashima, P.C. Yang, M.V. McConnell, D.G. Nishimura, H. Dai, Nat. Mater. 5 (2006) 971–976.
[5] R. Hergt, W. Andr¨a, C.G. d' Ambly, I. Hilger, W.A. Kaiser, U. Richter, H.-G. Schmidt, IEEE Trans. Magn. 34 (1998) 3745–3754.
[6] C. Desvaux, C. Amiens, P. Fejes, P. Renaud, M. Respaud, P. Lecante, E. Snoeck, B. Chaudret, Nat. Mater. 4 (2005) 750–753.
[7] L. Wang, F. He, Y. Wan, J. Alloys Compd. 509 (2011) 4726–4730.
[8] R.S. Sundar, S.C. Deevi, Int. Mater. Rev. 50 (2005) 157–192.
[9] D.I. Bardos, J. Appl. Phys. 40 (1969) 1371–1372.
[10] C. Kuhrt, L.1. Schultz, J. Appl. Phys. 73 (1993) 6588–6590.
[11] X. Gao, S.C. Tan, A.T.S. Wee, J. Wu, L. Kong, X. Yu, H.O. Moser, J. Electron Spectrosc. Relat. Phenom. 150 (2006) 11–14.
[12] G.S. Chaubey, C. Barcena, N. Poudyal, C.b. Rong, J. Gao, S. Sun, J.P. Liu, J. Am. Chem. Soc. 129 (2007) 7214–7215.
[13] D. Alloyeau, C. Ricolleau, C. Mottet, T. Oikawa, C. Langlois, Y. Le Bouar, N. Braidy, A.1. Loiseau, Nat. Mater. 8 (2009) 940–946.
[14] C. Desvaux, P. Lecante, M. Respaud, B. Chaudret, J. Mater. Chem. 20 (2010) 103–109.
[15] G.X. Chen, M.H. Hong, B. Lan, Z.B. Wang, Y.F. Lu, T.C. Chong, Appl. Surf. Sci. 228 (2004) 169–175.
[16] D. Ko, K.R. Poeppelmeier, D.R. Kammler, G.B. Gonzalez, T.O. Mason, D.L. Williamson, D.L. Young, T.J. Coutts, J. Solid State Chem. 163 (2002) 259–266.
[17] J.A. Gomes, M.H. Sousa, G.J. da Silva, F.A. Tourinho, J. Mestnik-Filho, R. Itri, G.de M. Azevedo, J. Depeyrot, J. Magn. Magn. Mater. 300 (2006) e213–e216.
[18] A.C. Larson, R.B. Von Dreele, General Structure Analysis System (GSAS), Los Alamos National Laboratory Report LAUR, 1994, 86–748.
[19] C.b. Rong, D. Li, V. Nandwana, N. Poudyal, Y. Ding, Z.L. Wang, H. Zeng, J.P. Liu, Adv. Mater. 18 (2006) 2984–2988.
[20] K.J. Carroll, D.M. Hudgins, L.W. Brown III, S.D. Yoon, D. Heiman, V.G. Harris, E.E. Carpenter, J. Appl. Phys. 107 (2010), 09A303.

[21] Pierre Villars, L.D. Calvert, W.B. Pearson, Pearson's Handbook of Crystallographic Data for Intermetallic Phases, ASM International, Materials Park, OH, 1991.
[22] M. Racuciu, D.E. Creang, A.1. Airinei, Eur. Phys. J. E 21 (2006) 117–121.
[23] X. Wu, P.L. Redmond, H. Liu, Y. Chen, M. Steigerwald, L. Brus, J. Am. Chem. Soc. 130 (2008) 9500–9506.
[24] L. Brus, Acc. Chem. Res. 41 (2008) 1742–1749.
[25] A. Goodarzi, Y. Sahoo, M.T. Swihart, P.N. Prasad, Mater. Res. Soc. Symp. – Proc. 789 (2003) 129–134.
[26] P.L. Redmond, X. Wu, L. Brus, J. Phys. Chem. C 111 (2007) 8942–8947.
[27] Xian-Wen Wei, Guo-Xing Zhu, Yuan-Jun Liu, Yong-Hong Ni, You Song, Zheng Xu, Chem. Mater. 20 (2008) 6248–6253.
[28] Daisuke Kodama, Kozo Shinoda, Kimitaka Sato, Yoshihiro Konno, R.J. Joseyphus, Kenichi Motomiya, Hideyuki Takahashi, Takatoshi Matsumoto, Yoshinori Sato, Kazuyuki Tohji, Balachandran Jeyadevan, Adv. Mater. 18 (2006) 3154–3159.
[29] J.C. Slater, J. Appl. Phys. 8 (1937) 385–390.
[30] L. Pauling, Phys. Rev. 54 (1938) 899–904.
[31] Sozhin Chikazumi, Physics of Ferromagnetism, second edition, Oxford University Press, New York, 1997.
[32] L. Dale, Huber, Small 1 (2005) 482–501.
[33] B.D. Cullity, C.D. Graham, Introduction to Magnetic Materials, second edition, John Wiley & Sons, Inc., Hoboken, New Jersey, 2009.
[34] Y.D. Yao, Y.Y. Chen, S.F. Lee, W.C. Chang, H.L. Hu, J. Magn. Magn. Mater. 239 (2002) 249–251.
[35] Toshikazu Tanaka, Nobuazki Tamagawa, Jpn. J. Appl. Phys. 6 (1967) 1096–1100.
[36] G. Herzer, IEEE Trans. Magn. 26 (1990) 1397–1402.
[37] S.D. Yoon, A.K. Baraskar, A. Geiler, A. Yang, C. Pettiford, N.X. Sun, R. Goswami, M.A. Willard, C. Vittoria, V.G. Harris, J. Appl. Phys. 103 (2008) 063917.
[38] R. Skomski, J. Phys.: Condens. Matter 15 (2003) R841–R896.
[39] M. Hesani, A. Yazdani, B. Abedi Ravan, M. Ghazanfari, Solid State Commun. 150 (2010) 594–597.
[40] Bernard Barbara, Solid State Sci. 7 (2005) 668–681.
[41] K. Santosh, D. Pal, Bahadur, Mater. Lett. 64 (2010) 1127–1129.